Lab on a Chip

TECHNICAL INNOVATION

View Article Online
View Journal | View Issue

Cite this: *Lab Chip*, 2015, **15**, 1004

A novel fluidic control method for nanofluidics by solvent–solvent interaction in a hybrid chip†

Guangchun Fu,‡[a] Zezhi Zheng,‡[a] Xin Li,[a] Yue Sun[b] and Hong Chen*[a]

Received 20th October 2014,
Accepted 22nd December 2014

DOI: 10.1039/c4lc01241k

www.rsc.org/loc

The fluidic control method is a fundamental technology for the development of nanofluidics. In this report, an organic phase was driven to flow inside the nanochannel because of its dissolution into an aqueous phase. With selective modification, a stable organic/aqueous interface was generated at the junction of the micro/nanochannels in a hybrid chip. The aqueous phase was kept flowing in the microchannel, and the organic phase in the nanochannel dissolved into the aqueous phase through the interface and produced a flow inside the nanochannel. This method is simple, easy to control and requires no specific equipment. Importantly, the flow is driven by the surface tension in a controllable manner, which will not be affected by the depth of the nanochannel. This method can be a useful alternative to the present fluidic control methods in nanofluidics.

Introduction

Over the past decades, microfluidics and the micro total analysis system (μTAS) have been extensively developed for various applications with merits including large surface-to-volume ratio, fast transfer and high throughput.[1,2] With the progress in nanofabrication and nanotechnology, nanofluidics is gaining more attention and interest due to its prominent and specific characteristics. Many applications have been developed based on these properties.[3–9] Recently, several reviews have been published to introduce the fabrication, fluidic control method, detection, specific properties, transport and applications of nanofluidics.[10–20]

The fluidic control method is a fundamental and important technology for the development of nanofluidics. Different fluidic control methods have been applied in nanofluidics, such as electric field driven, pressure driven, entropy driven,[4,21] shear driven[22,23] and evaporation driven methods.[24,25] The electric field driven technique is the most used method. It has been used in controlled injection,[26] fluid dispensing,[27] oligonucleotide separation[28] and electrophoretically driven transport[29] in nanofluidics. The electric field driven method has also been utilized to generate the electroosmotic flow in porous anodic alumina membranes.[30,31] However, when the dimensions of the nanochannel approach the Debye length, the profile of the potential becomes parabolic. This is different from that involving microchannels, so the electric field driven method should not be simply applied in nanofluidics as it was in microfluidics. The charged surface will also affect the existence of ions and transfer in the nanochannel. However, ion-enrichment and ion-depletion effects were realized by utilizing this phenomenon.[32] Another disadvantage of the electric field driven method is that it can only be used in aqueous solutions.[33]

The pressure driven method is another often-used method in nanofluidics. According to the Hagen–Poiseuille law, the pressure drop in the laminar flow without slip flow in a circular pipe is theoretically expected to increase with decreasing d^4 (where d is the equivalent diameter of the channel).[34] The pressure needed to overcome the fluidic resistance is much higher in a nanochannel than in a microchannel. The syringe pumps used in microfluidics cannot provide the required pressure under the ultra-small volume flow rate in the nanochannel. Many methods have been developed to apply pressure indirectly on the nanochannels. Kitamori *et al.* applied liquid pressure on the nanochannel using a back pressure regulator.[33] Bai *et al.* also indirectly applied the pressure between the two ends of the nanochannel by two pressure regulators.[35] Air-pressure-based nanofluidic control systems have been developed to achieve better performance and regulation.[36,37] Hydrodynamics has also been adopted to manipulate DNA in the nanochannel.[38] Usually, a pressure control equipment is needed for the pressure driven method. And in the above applications, in which most of the samples flowed

[a] *School of Physics and Mechanical & Electrical Engineering/Pen-Tung Sah Institute of Micro-Nano Science and Technology, Xiamen University, Xiamen 361005, PR China. E-mail: hongc@xmu.edu.cn; Fax: +86 592 2187196; Tel: +86 592 2181340*

[b] *College of Traditional Chinese Medicine, Guangdong Pharmaceutical University, Guangzhou 510006, PR China*

† Electronic supplementary information (ESI) available. See DOI: 10.1039/c4lc01241k

‡ Both authors contributed equally to this work.

away through the microchannel, only a very small amount of the sample was utilized.

Here, the dissolution of an organic phase into an aqueous phase was demonstrated at the junction of the micro/nanochannels. This phenomenon has been reported to be used for liquid–liquid extraction in microchannels,[39,40] now it can also be used as a new fluidic control method for nanofluidics. The organic phase can be driven to flow through the nanochannel. Most of the sample can be utilized in the nanochannel, making it suitable for expensive or precious samples. As an alternative to the present methods, this method is simple, easy to control, requires no special equipment and, importantly, is not affected by the depth of the nanochannel.

Methods

Standard UV photolithography, wet chemical etching and room temperature bonding have been used to fabricate the hybrid microfluidic chip with micro/nanochannels.[41] As shown in Fig. 1a, the V-shaped channel in green is the microchannel (400 μm in width and 25 μm in depth), and the I-shaped channel in purple is the nanochannel with a depth from tens to hundreds of nanometers (400 μm in width). Details of the fabrication are described in the ESI.†

The nanochannel was selectively modified by a silanizing reagent and became hydrophobic, whereas the microchannel was unmodified and remained hydrophilic. 10% dimethyldichlorosilane in hexyl alcohol was introduced into the nanochannel and held for 20 min. At the same time, 5% sodium hydroxide flowed through the microchannel intermittently. After the pretreatment, the channels were cleaned with acetone and DI water until there was no debris left. Then, the microfluidic chip was incubated at 110 °C for 1 h.

As shown in Fig. 1a, the organic phase (hexyl alcohol) was introduced and filled the entire nanochannel by capillary force through the organic phase reservoir. The aqueous phase was flowed through the microchannels by a syringe pump.

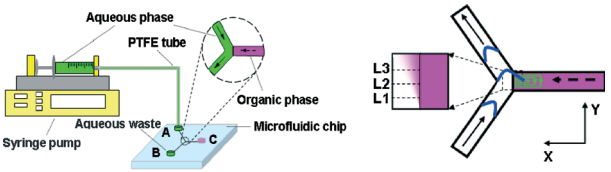

Fig. 1 (a) The schematic diagram showing how the organic phase dissolved into the aqueous phase and generated flow inside the nanochannel. (b) The organic phase dissolved into the aqueous phase and generated a concentration gradient in the aqueous phase. The concentration gradient developed at the different positions (L_1, L_2 and L_3), when the aqueous phase flowed along the microchannels. To highlight the organic phase's concentration gradient, only the organic phase is shown in color. The solid arrow shows the pressure driven flow of the aqueous phase, and the blue curves show its parabolic profile. The dashed arrow shows the flow of the organic phase caused by the dissolution. The green rings show the circular flow near the interface.

The aqueous and organic phases formed a stable interface at the junction between the micro/nanochannels. R6G was already dissolved in the solvents to illuminate the two phases and their interface. The syringe pump kept the aqueous phase flowing along the microchannels, and the organic phase was dissolved in and removed by the aqueous phase. The dissolved organic phase was compensated for by the organic phase in the reservoir, so there was a flow of the organic phase inside the nanochannel toward the junction.

Results and discussion

Design and theory

In this design, the organic phase dissolved into the aqueous phase and generated a flow inside the nanochannel. The flow rate of the organic phase was determined by the dissolution rate of the organic phase into the aqueous phase. As shown in Fig. 1b, the dissolved organic phase generated a concentration gradient in the aqueous phase in the direction normal to the interface (X axis). In the direction of the aqueous phase flow (Y axis), the concentration gradient also developed. This meant that the organic phase diffused deeper into the main body of the aqueous phase when the aqueous phase flowed forward (as L_1, L_2 and L_3 in Fig. 1b). By integrating all of these concentration gradients, the dissolution rate of the organic phase can be calculated, and the flow rate of the organic phase in the nanochannel was also available.

At the interface, the organic phase saturated the aqueous phase, and its concentration was constant (C). Because the aqueous phase flowed along the interface for less than several seconds, there was not enough time for the dissolved organic phase to reach the other wall of the microchannel. The unsteady diffusion in the X axis can be described as follows:

$$\frac{\partial c}{\partial t} = \frac{v_1 \partial c}{\partial y} = -\left\{ \frac{j\big|_{x+\Delta x} - j\big|_x}{(x+\Delta x) - x} \right\} \quad (1)$$

where c is the concentration of the dissolved organic phase at point x in the X axis, and j is the flux along the X axis. v_1 is the flow rate of the aqueous phase at the two-phase interface.

When the parabolic laminar flow profile of the pressure driven flow is considered, the average flow rate of the organic phase inside the nanochannel (v_2) is calculated by using the equation:

$$v_2 = 2VC\sqrt{\frac{2D}{l\pi}\left[1 - \left(\frac{r}{R}\right)^2\right]v} \quad (2)$$

where V is the unit volume of the organic phase, D is the diffusion coefficient, l is the length of the interface, r is the distance from the position with the maximum flow rate in the microchannel to the interface, R is the distance from the position with the maximum flow rate in the microchannel to the position with the flow rate of 0 in the circular flow and v is

the average flow rate of the aqueous phase in the microchannel. The details of the simulation are described in the ESI.†

The flow rate of the organic phase in the nanochannel was decided by the average flow rate of the aqueous phase in the microchannels. The organic phase's diffusion coefficient and solubility in the aqueous phase also increased its flow rate. A longer interface length helped to dissolve more organic phase into the aqueous phase, but the average flow rate of the organic phase decreased. The diffusion time of the organic phase is proportional to the square of the diffusion distance. The flux along the interface decreased with increasing interface length, so the average flow rate of the organic phase for the whole cross-sectional area also decreased with increasing interface length. The depth of the channel did not appear in the final equation, indicating that the channel's depth had no effect on the flow rate. This was because of the fact that the organic phase was driven by the surface tension between the two-phase interface. Compared with other pressure driven methods, the flow resistance in this design did not increase with the decrease in the channel's dimensions. Theoretically, this method can be used for channels on any scale.

Selective modification and characterization

To realize the solvent's dissolution, a stable interface must be formed between the organic and aqueous phases at the junction of the micro/nanochannels. Without the interface, there will be a pressure drop between the two ends of the nanochannel. As shown in Fig. S5,† the solvent in the nanochannel was indirectly driven to flow toward the other end of the nanochannel. Because the glass's surface was hydrophilic, the aqueous phase tended to flow into the nanochannel. Selective modification was performed to make the nanochannel hydrophobic, which helped to generate a stable two-phase interface. The modification was first performed on a glass slide to optimize the conditions. The static contact angle was measured to quantify the effects. The concentration of dimethyldichlorosilane and the treatment time were investigated, as shown in Fig. S6a and b.† As shown in Fig. S7a,† the contact angle of DI water (2 μL) increased from 31.29° ± 0.98° to 83.32° ± 0.85° with the help of the treatment. The effect on hexyl alcohol is also shown in Fig. S7b.† Before the modification, the contact angle of hexyl alcohol (25.07° ± 0.42°) was close to that of DI water, indicating that the water could easily flow into the nanochannel. However, hexyl alcohol's contact angle decreased to 19.21° ± 0.86° after the modification, which was much smaller than that of DI water. This provided a much stronger force to prevent the DI water from flowing into the nanochannel after modification.

The modification was then performed on the nanochannel's surface for 20 min. During the modification, 5% sodium hydroxide solution was flowed through the microchannel several times to hydrolyze the dimethyldichlorosilane that flowed into the microchannels. In this way, the nanochannel's surface was hydrophobic, whereas the microchannel's surface was still hydrophilic. Fig. S7c† shows the effect of the selective modification. The left side shows the microchannel and DI water flowing through it. The right side is the nanochannel already filled with the organic phase. Without the selective modification, the water flowed into the nanochannel several minutes after the two-phase interface was generated and produced the light area in the nanochannel near the junction (because R6G tended to dissolve and be extracted in hexyl alcohol). With the selective modification, the water did not flow into the nanochannel. The interface was very stable and can be maintained for several days.

Here, the surface tension was utilized to maintain the two-phase interface and acted as the driving force. The force provided by the surface tension is calculated by the equation:

$$F = \gamma L \cos\theta \tag{3}$$

where γ is the surface tension, L is the contact length and θ is the contact angle. In order to get the contact angle in this design (hexyl alcohol/water on the modified surface), the two-phase interface was generated in a modified capillary with a square cross section (the length of a side is 1 mm). The contact angle was measured to be 62°, and the force generated by the two-phase interface in the microfluidic chip was calculated to be $3.76 \times 10^{-4}\gamma$ N. By the contact angle and surface tension, the organic phase can be optimized to provide the interface which is stable enough.

The solvent's flow inside the nanochannel

After the selective modification, the nanochannel was filled with the organic phase. The aqueous phase was introduced into the microchannel and kept flowing. The organic phase near the interface dissolved into the aqueous phase and was removed, which induced the organic phase to flow toward the junction inside the nanochannel. To illuminate and investigate the organic phase's flow, a section of the aqueous phase was introduced into the organic phase inside the nanochannel (as shown in the inset of Fig. 2a). The interface kept moving left where the junction was (as shown in Fig. 2b), which meant that the organic phase in the nanochannel was flowing toward the junction of the micro/nanochannels. The effect of the different flow rates of the aqueous phase is shown in Fig. 2a. When the flow rate of the aqueous phase increased from 0 to 8 mm s^{-1}, the flow rate of the organic phase also increased from 2.27 μm s^{-1} to 8.7 μm s^{-1} (the regression equation was $Y = 3.7205X^{0.4292}$, $R^2 = 0.9789$). The experimental data and theory expectation ($Y = 3.7205X^{0.5}$) are both plotted in Fig. 2a, in which the same coefficient (3.7205) was adopted in the theory expectation. When the aqueous phase stopped flowing, the expectation flow rate of the organic phase decreased quickly and then became 0, because it assumed that all aqueous phase near the interface had already been saturated by the organic phase. In the

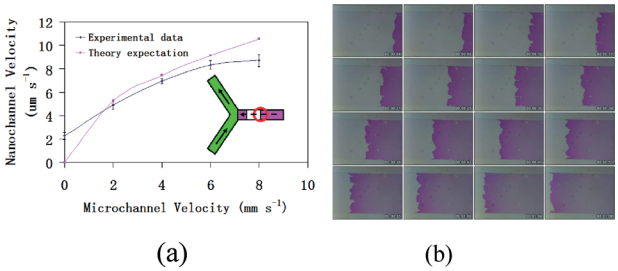

Fig. 2 (a) The relationship between the flow rates of the organic phase in the nanochannel and the aqueous phase in the microchannel. The inset shows the diagram of the process. A section of the aqueous phase (the white area in the nanochannel) was introduced into the nanochannel to illuminate the organic phase's flow. The interface in the ESI† video and in (b) is the position indicated by the red circle. (b) A series of images showing the flow inside the nanochannel. The solution in white is the aqueous phase, and the solution in purple is the organic phase. The movement of the interface proved that the organic phase in the nanochannel was flowing toward the micro/nanochannel junction. The total time for these images was approximately 1 min, and the width of the channel was 400 μm.

experiment, the organic phase had a flow rate of 2.27 μm s^{-1}. The organic phase was still dissolving into the aqueous phase, because the aqueous phase actually had not been saturated. With a flow rate of 2.27 μm s^{-1}, the dissolved organic phase per second can saturate the aqueous phase with a volume of 5.9×10^{-15} m^3, which corresponds to the volume inside the microchannel with a length of 0.59 μm. Theoretically, the flow rate of the organic phase can be maintained for tens of minutes.

This design was also used to measure the dynamic quenching of the fluorescence under different pH conditions. HCl solutions with different pH values were driven into the microchannel with a flow rate of 0.5 mm s^{-1}. Hexyl alcohol with fluorescein flowed into the nanochannel. When the organic phase dissolved into the aqueous phase, the fluorescein also dissolved into the aqueous phase and flowed downstream. Fluorescein fluorescence was found near the right wall of the microchannel. When the pH values were 2.12 and 3.31, the fluorescence was totally quenched (as shown in Fig. S8a and b†). With the increase in the pH value, the fluorescein fluorescence increased. The fluorescence intensity under the different pH conditions was measured at the position indicated by the yellow circle in Fig. 3a (100 μm downstream from the interface). The relationship between the pH value and the fluorescence intensity is shown in Fig. 3b. With this design, other dynamic parameters (diffusion coefficient and quenching rate) can also be obtained. This design can also be used in applications involving fast reactions.

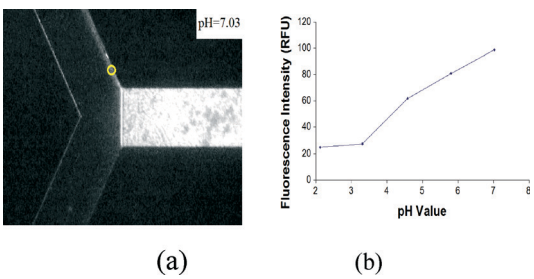

Fig. 3 (a) The fluorescein's fluorescence when the pH value was 7.03. (b) The fluorescence intensities under the different pH conditions at the position indicated by the yellow circle in (a).

Conclusions

A phenomenon of the solvent's dissolution at the junction between the micro/nanochannels was reported and used as a new fluidic control method to drive the flow of the organic phase in a nanochannel. This fluidic control method is simple and requires no expensive and elaborate equipment. The flow rate in the nanochannel is not related to the depth of the channel, so this method can be applied in nanochannels with any depth. There is no need to consider the pressure drop, which increases greatly with decreasing channel dimensions. Instead of modifying the nanochannel, the aqueous phase can also be driven to flow inside the nanochannel by modifying the microchannel. To satisfy the requirements of other applications, an organic phase with different solubilities in the aqueous phase can be used to determine the flow rate on different scales. Therefore, this method is a useful alternative to the present methods in nanofluidics.

Acknowledgements

We gratefully acknowledge support from the National Natural Science Foundation of China (grant 21005066, 81001600 and 21203159).

Notes and references

1 G. M. Whitesides, *Nature*, 2006, **442**, 368–373.
2 P. Yager, T. Edwards, E. Fu, K. Helton, K. Nelson, M. R. Tam and B. H. Weigl, *Nature*, 2006, **442**, 412–418.
3 D. Huh, K. L. Mills, X. Zhu, M. A. Burns, M. D. Thouless and S. Takayama, *Nat. Mater.*, 2007, **6**, 424–428.
4 J. Han, *Science*, 2000, **288**, 1026–1029.
5 V. R. Dukkipati, J. H. Kim, S. W. Pang and R. G. Larson, *Nano Lett.*, 2006, **6**, 2499–2504.
6 C. H. Reccius, J. T. Mannion, J. D. Cross and H. Craighead, *Phys. Rev. Lett.*, 2005, **95**, 268101.
7 D. Gillespie, *Nano Lett.*, 2012, **12**, 1410–1416.
8 C. Davidson and X. Xuan, *Electrophoresis*, 2008, **29**, 1125–1130.
9 M. Krishnan, N. Mojarad, P. Kukura and V. Sandoghdar, *Nature*, 2010, **467**, 692–695.
10 W. Sparreboom, A. Van Den Berg and J. Eijkel, *Nat. Nanotechnol.*, 2009, **4**, 713–720.
11 K. Mawatari, Y. Kazoe, H. Shimizu, Y. Pihosh and T. Kitamori, *Anal. Chem.*, 2014, **86**, 4068–4077.
12 A. Piruska, M. Gong, J. V. Sweedler and P. W. Bohn, *Chem. Soc. Rev.*, 2010, **39**, 1060–1072.
13 T. Tsukahara, K. Mawatari and T. Kitamori, *Chem. Soc. Rev.*, 2010, **39**, 1000–1013.

14 J. C. T. Eijkel and A. V. D. Berg, *Microfluid. Nanofluid.*, 2005, **1**, 249–267.
15 P. Abgrall and N. T. Nguyen, *Anal. Chem.*, 2008, **80**, 2326–2341.
16 R. Chantiwas, S. Park, S. A. Soper, B. C. Kim, S. Takayama, V. Sunkara, H. Hwang and Y. K. Cho, *Chem. Soc. Rev.*, 2011, **40**, 3677–3702.
17 S. Pennathur and J. G. Santiago, *Anal. Chem.*, 2005, **77**, 6772–6781.
18 M. Napoli, J. C. Eijkel and S. Pennathur, *Lab Chip*, 2010, **10**, 957–985.
19 D. Mijatovic, J. C. Eijkel and A. Van Den Berg, *Lab Chip*, 2005, **5**, 492–500.
20 K. Mawatari, T. Tsukahara, Y. Sugii and T. Kitamori, *Nanoscale*, 2010, **2**, 1588–1595.
21 J. W. Yeh, A. Taloni, Y. L. Chen and C. F. Chou, *Nano Lett.*, 2012, **12**, 1597–1602.
22 S. Vankrunkelsven, D. Clicq, D. Cabooter, W. De Malsche, J. G. Gardeniers and G. Desmet, *J. Chromatogr. A*, 2006, **1102**, 96–103.
23 S. De Bruyne, W. De Malsche, V. Fekete, H. Thienpont, H. Ottevaere, H. Gardeniers and G. Desmet, *Analyst*, 2013, **138**, 6127–6133.
24 M. N. Hamblin, J. Xuan, D. Maynes, H. D. Tolley, D. M. Belnap, A. T. Woolley, M. L. Lee and A. R. Hawkins, *Lab Chip*, 2010, **10**, 173–178.
25 J. Eijkel, B. Dan, H. Reemeijer, D. Hermes, J. Bomer and A. Van Den Berg, *Phys. Rev. Lett.*, 2005, 95.
26 A. L. Garcia, L. K. Ista, D. N. Petsev, M. J. O'Brien, P. Bisong, A. A. Mammoli, S. R. Brueck and G. P. Lopez, *Lab Chip*, 2005, **5**, 1271–1276.
27 M. L. Kovarik and S. C. Jacobson, *Anal. Chem.*, 2007, **79**, 1655–1660.
28 D. E. Huber, M. L. Markel, S. Pennathur and K. D. Patel, *Lab Chip*, 2009, **9**, 2933–2940.
29 L. D. Menard and J. M. Ramsey, *Anal. Chem.*, 2013, **85**, 1146–1153.
30 W. Chen, J. H. Yuan and X. H. Xia, *Anal. Chem.*, 2005, **77**, 8102–8108.
31 S. J. Li, C. Wang, Z. Q. Wu, J. J. Xu, X. H. Xia and H. Y. Chen, *Chem. – Eur. J.*, 2010, **16**, 10186–10194.
32 Q. Pu, J. Yun, H. Temkin and S. Liu, *Nano Lett.*, 2004, **4**, 1099–1103.
33 E. Tamaki, A. Hibara, H. B. Kim, M. Tokeshi and T. Kitamori, *J. Chromatogr. A*, 2006, **1137**, 256–262.
34 K. Mawatari, T. Tsukahara, Y. Sugii and T. Kitamori, *Nanoscale*, 2010, **2**, 1588–1595.
35 Q. Wu, J. T. Ok, Y. Sun, S. T. Retterer, K. B. Neeves, X. Yin, B. Bai and Y. Ma, *Lab Chip*, 2013, **13**, 1165–1171.
36 T. Tsukahara, K. Mawatari, A. Hibara and T. Kitamori, *Anal. Bioanal. Chem.*, 2008, **391**, 2745–2752.
37 K. Mawatari, S. Kubota, Y. Xu, C. Priest, R. Sedev, J. Ralston and T. Kitamori, *Anal. Chem.*, 2012, **84**, 10812–10816.
38 Q. He, H. Ranchon, P. Carrivain, Y. Viero, J. Lacroix, C. Blatché, E. Daran, J. M. Victor and A. Bancaud, *Macromolecules*, 2013, **46**, 6195–6202.
39 H. Chen, Q. Fang, X. F. Yin and Z. L. Fang, *Lab Chip*, 2005, **5**, 719–725.
40 M. Sun, W. B. Du and Q. Fang, *Talanta*, 2006, **70**, 392–396.
41 Q. He, S. Chen, Y. Su, Q. Fang and H. Chen, *Anal. Chim. Acta*, 2008, **628**, 1–8.

